ELSEVIER

Journal of Alloys and Compounds 459 (2008) 425–432

Journal of ALLOYS AND COMPOUNDS

www.elsevier.com/locate/jallcom

Structural characterization and hydrogen sorption properties of nanocrystalline Mg_2Ni

F.C. Gennari [a,b,*], M.R. Esquivel [a,b,c]

[a] *Consejo Nacional de Investigaciones Científicas y Técnicas, CONICET, Centro Atómico Bariloche (CNEA), R8420AGP, S.C. de Bariloche, Río Negro, Argentina*

[b] *Instituto Balseiro (UNCuyo and CNEA), Centro Atómico Bariloche (CNEA), R8420AGP, S.C. de Bariloche, Río Negro, Argentina*

[c] *Comisión Nacional de Energía Atómica (CNEA), Centro Atómico Bariloche (CNEA), R8420AGP, S.C. de Bariloche, Río Negro, Argentina*

Received 3 April 2007; accepted 24 April 2007
Available online 29 April 2007

Abstract

The structure, chemical distribution, microstructure and thermal stability of a 2Mg–Ni mixture milled at different times in a low energy ball mill were investigated. After short time processing, a mixture of amorphous Mg-rich phase, nanocrystalline Mg and crystalline Ni was obtained. The crystallite size reduction and strain increment along with the formation of an amorphous phase was associated to the refinement of Mg at this stage. After long time milling, nanocrystalline Mg_2Ni was produced and both amorphous Mg-rich phase and Ni remained in the mixture as residual phases. Stable nanocrystalline Mg_2Ni was successfully synthesized by a combination of low energy mechanical alloying and further non-isothermal heating up to 300 °C. The reactivity and equilibrium features of Mg_2Ni were characterized by both hydrogen absorption/desorption and pressure–composition isotherm measurements. The nanostructured intermetallic showed a 3.0 wt% hydrogen storage capacity without activation and excellent hydrogen absorption/desorption kinetics.

Keywords: Hydrogen storage materials; Mechanical alloying; Intermetallics; Nanocrystalline materials; Mg_2Ni

1. Introduction

The ternary hydrides of the Mg_xTH_y (T: transition metal) family represent a promising alternative as hydrogen storage materials. Noteworthy of study are Mg_2FeH_6, Mg_2CoH_5 and Mg_2NiH_4 due to their respective high storage capacity values of 5.5, 4.5 and 3.6 wt% along with high volumetric hydrogen density comprised between 100 and 150 kg H^2 m^{-3} and low cost. However, single-phase hydrides of this family are not easy to produce mainly because of either the absence of a precursor alloy such as Mg_2Co or Mg_2Fe or a large difference between the melting points of the metals [1,2].

Two stable intermetallics, Mg_2Ni and $MgNi_2$, have been reported in the Mg–Ni system [1]. While $MgNi_2$ does not absorb hydrogen, Mg_2Ni forms Mg_2NiH_4. This hydride has a lower capacity than MgH_2 (3.6 wt%) but faster hydriding kinetics [3]. Mg_2NiH_4 possesses a high temperature (HT) cubic and a low temperature (LT) monoclinic structure [4,5]. The first one transforms into the second one on cooling. LT hydride structure is difficult to obtain by direct hydrogenation under moderate pressure conditions while HT hydride structure is easily produced by hydrogenation of Mg_2Ni at high temperature [4,6].

Melting is the traditional technique to produce Mg_2Ni. However, the large differences in the melting point and vapor pressure between the constituents make difficult the synthesis of a high quality intermetallic. Nevertheless, this goal is fulfilled by additional processing such as re-melting, Mg addition or annealing below the peritectic temperature. An alternative for synthesizing Mg_2Ni is the use of the mechanical alloying (MA) process [6]. This technique is commonly utilized to obtain a high variety of materials including intermetallics, ceramics, solid solutions and metastable phases such as amorphous alloys and supersaturated solutions [7]. It overcomes many of the limitations of conventional alloying processes and has the advantage of cre-

* Corresponding autor at: Centro Atómico Bariloche (CNEA), R8420AGP, S.C. de Bariloche, Río Negro, Argentina. Tel.: +54 2944 445118; fax: +54 2944 445190.

E-mail addresses: gennari@cab.cnea.gov.ar (F.C. Gennari), esquivel@cab.cnea.gov.ar (M.R. Esquivel).

0925-8388/$ – see front matter © 2007 Elsevier B.V. All rights reserved.
doi:10.1016/j.jallcom.2007.04.283

ating true alloys of metals and non-metal composites that are difficult to combine otherwise. The cycle of fracture and cold welding occurring during the MA of the metals mixture induces an increase of the amount of surface defects and a reduction in the crystallite size to the nanometer range [7]. These parameters are relevant to reduce hydrogen pressure, temperature and activation time, to improve hydrogen absorption/desorption kinetics and to increase the absorption capacity of a specific material. Therefore, MA process can be considered a powerful technique to produce hydrogen-absorbing alloys with enhanced properties [6].

Intermetallic Mg_2Ni has been successfully formed using mainly high energy milling [6,8–16]. Huot et al. [8] showed that MA of the 2Mg–Ni mixture leads to the Mg_2Ni formation and the stationary state was reached after 22 h. The authors mentioned that the MA process was not very effective and it only occurred on the powder surface. Singh et al. [10] observed the Mg_2Ni formation with some free Ni after 100 h of milling. After activation, the maximum hydrogen storage capacity reached was 3.2 wt%. Zaluski et al. [6] formed nanocrystalline Mg_2Ni by MA using high energy mill and high ball-to-powder mass ratio. The ball milled material absorbed hydrogen with no activation reaching a final hydrogen content between 3 and 3.4 wt%. Chen et al. [12] obtained crystalline Mg_2Ni after 14 h of milling. Further processing produced intermetallic amorphization. Research in most recent works has been oriented to optimize the Mg_2Ni synthesis procedure by modification of milling parameters [13–15]. Only two investigations analyzed the hydrogen sorption properties of the milled materials [13,16]. Abdellaoui et al. [13] studied the hydrogen sorption of the milled materials after activation by thermal treatment, showing the best hydrogen absorption capacity reported (3.5 wt%). Spassov et al. [16] characterized hydrogen desorption behavior of nanocrystalline/amorphous phases obtained after high energy milling and the hydrogen storage capacity was about 2.2 wt% at 220 °C. Despite all the research done, there still is a lack of research on the ball milling of Mg–Ni mixture using low energy milling, except for the work by Aymard et al. [17]. These authors detected a mixture consisting of an amorphous phase and pure Ni after 200 h of milling. They suggested that the amorphous phase consisted of Mg_2Ni and nanocrystalline Mg. Complete Mg_2Ni formation was observed after 20 h of thermal treatment at 300 °C. No measurements on hydrogen absorption/desorption properties were reported.

In the present study, the 2Mg–Ni mixture was mechanically alloyed using a low energy mill to produce nanocrystalline Mg_2Ni and to characterize their hydrogen storage properties. The MA process leads to the formation of a Mg-rich amorphous phase, residual Ni and/or nanocrystalline Mg_2Ni as a function of milling time. The annealing up to 300 °C of the MA samples – an interesting temperature for hydrogen absorption/desorption from Mg_2Ni – introduces relevant microstructural and structural modifications in the phases detected. The goal of this study is to produce nanocrystalline Mg_2Ni by combination of MA process and annealing, which exhibits good hydrogen absorption/desorption properties without activation. This research is part of a wider project oriented to obtain some fundamental knowledge of the physicochemical behavior of the Mg–Ni, Mg–Co and Mg–Fe systems in the presence of hydrogen [18–20].

2. Experimental

The mechanical alloying processes were carried out using a Uni-Ball-Mill II apparatus (Australian Scientific Instrument). A mixture of pure magnesium (99.9%) and nickel powders (99.99%) with an atomic proportion of 2:1 was introduced into a stainless steel container together with ferromagnetic steel balls. All handling of the powders was performed in a glove box under purified argon atmosphere. The mixtures were milled for different times up to a total of 320 h. The milling processes proceeded in a stationary argon atmosphere. The ball-to-powder weight ratio selected was 42:1.

At regular intervals, the container was opened in an argon dry box and a small amount of powder was withdrawn for analysis by X-ray powder diffraction (XRD), scanning electron microscopy with energy-dispersive X-ray analyzer (SEM–EDX) and differential scanning calorimetry (DSC). The structural evolution during MA and subsequent annealing was investigated by XRD (Philips PW 1710/01 Instruments) using Cu Kα radiation (graphite monochromator). Strain and crystallite size effects were estimated from diffraction peaks by assuming empirically a Gauss and Cauchy (Lorentz) components distribution [21].

The morphological, chemical and microstructural characterizations were performed with SEM (SEM 515, Philips Electronic Instruments) and EDX on resin-mounted and polished samples. The thermal behavior of the samples was studied by DSC (DSC 2910, TA Instruments) using 5 °C min^{-1} of heating rate and 122 ml min^{-1} argon flow rate.

Dynamic pressure–composition isotherms (PCI) and hydrogen sorption kinetics were obtained using a modified Sieverts-type device, coupled with a mass flow controller [22]. Each sample was heated up to the reaction temperature under vacuum and kept at this temperature for 30 min before hydrogen reaction.

3. Results and discussion

3.1. Intermetallic formation: microstructural, structural and thermal analysis

The evolution of the 2Mg–Ni mixture as a function of milling time is presented in Fig. 1. A mixture of elemental Mg and Ni is clearly observed after 10 h of milling. JCPDS Powder Diffraction Data Reference Card Nos. 04-0850 and 35-0821

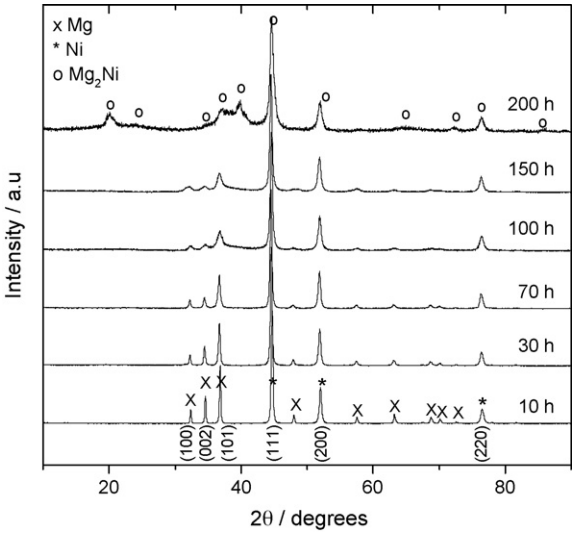

Fig. 1. X-ray diffraction patterns of the 2Mg–Ni mixture after MA as a function of milling time.

were assigned to cubic Ni and hexagonal Mg, respectively. As milling time is increased, diffraction peak intensity and width are reduced and augmented, respectively. The correlation between these effects and changes on the crystallite size and strain is summarized in Table 1. A noticeable broadening of the Mg peaks attributable to the reduction of the crystallite size and plastic deformation is observed at milling times higher than 70 h. At milling times higher than this value, the diffractograms exhibit a broad bump between 30° and 40° evidencing the formation of an amorphous phase. Unlike the evolution of Mg, changes on the Ni peaks are less evident up to 100 h of milling. Further milling only produces slight structural changes on Ni as observed on (1 1 1) and (2 0 0) diffraction peaks. The peak broadening and intensity lowering associated to crystallite size reduction and strain increase for the Ni phase are also shown in Table 1.

Table 1
Evolution of the average crystallite size d (nm) and average strain (%) of the different phases with the milling time

Milling time (h)	Mg		Ni		Mg_2Ni	
	d (nm)	Strain (%)	d (nm)	Strain (%)	d (nm)	Strain (%)
10	68	4	53	3	–	–
70	54	6	50	4		
100	25	10	49	4	–	–
150	18	14	43	4	–	–
200	–	–	27	8	16	28

After 200 h of milling, Mg(1 0 0), (0 0 2) and (1 0 1) diffraction lines evolve as a one broad bump and the formation of Mg_2Ni intermetallic phase (JCPDS Powder Diffraction Data Card No. 35-1225) is detected. At this stage of milling, a mix-

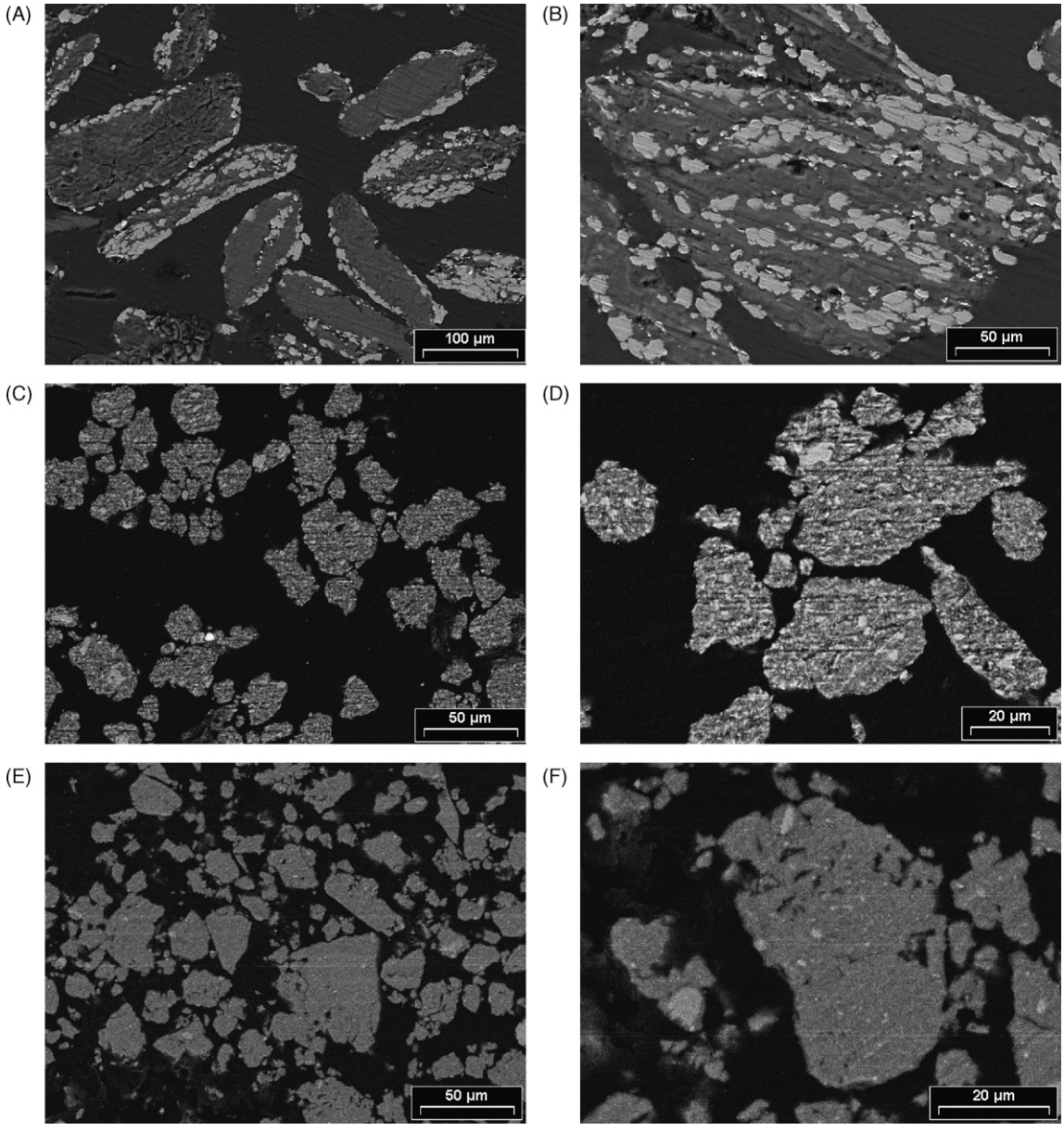

Fig. 2. SEM backscattered electron images after milling for 10 h (A and B), 100 h (C and D) and 200 h (E and F). Distribution of the agglomerate sizes (A, C and E) and agglomerate details (B, D and F).

ture of nanocrystalline Mg_2Ni, nanocrystalline Mg-rich phase and Ni is observed. No changes on the phases are detected by further milling up to 320 h (not shown here). Neither $MgNi_2$ nor MgO diffraction peaks were found after 320 h of MA. The formation of nanocrystalline Mg_2Ni after 200 h of milling is most likely associated to the crystallization of an amorphous phase produced as a consequence of long time MA as assessed in the next paragraphs.

SEM images of 2Mg–Ni mixture milled 2 h (A and B), 100 h (C and D) and 200 h (E and F) obtained with backscattered electrons are shown in Fig. 2. Darker and brighter zones are associated to Mg and Ni, respectively. As milling progresses, the agglomerate size decreases from 100–150 to 5–50 μm as displayed in Fig. 2A, C and E. The evolution of the Mg–Ni distribution as milling time increases is displayed in agglomerate details observed in Fig. 2B, D and F. Typical ductile–ductile couple lamellar structure is present at the beginning of the process (Fig. 2B). Milling progression incorporates Ni particles of sizes up to 30 μm into the Mg matrix. This process and refinement of the microstructure are enhanced as the cycle of fracturing and cold welding continues as shown in Fig. 2D. At this stage, Ni particles of sizes smaller than 5 μm are still identified into Mg matrix. Further milling increases the degree of mixing between Mg and Ni and it is practically impossible to differentiate richer zones of either element. Ni particle size is now reduced to values smaller than 1 μm, with exception of some clusters. It is in agreement with EDX analysis shown in Table 2. These measurements were performed on the dark area of agglomerates after different milling times. From these series of values, it is deduced that Mg matrix incorporates Ni as milling time increases, approaching the nominal composition of Mg_2Ni at 70 h of milling. As an interesting result, crystalline Mg_2Ni formation is not observed in XRD pattern at this milling time. However, the existence of an amorphous phase is evidenced in Fig. 1. This phase can be constituted by a Mg-rich phase Ni content is increased as milling evolves as indicated by the results shown in Table 2.

Thermal stabilities of the 2Mg–Ni powders after MA were investigated using a combination of DSC followed by XRD analysis. A unique thermal behavior during MA evolution is observed in Fig. 3. It is described by the presence of two exothermal peaks shown in DSC curves of this Figure. The first one appears between 100 and 150 °C. The second one occurs in a wider temperature zone ranging from either 150 °C or higher to 400 °C or higher temperatures. Each event is characterized by a decrease of temperature as milling time increases. This effect is stronger for the second peak showing a decrease in both starting and finishing temperatures. As displayed in Table 1 and Fig. 1, the presence of nanocrystalline Mg_2Ni before heating can be related to the minor temperature differences observed for the sample milled 200 h.

Table 2
EDX analysis performed on dark area from SEM backscattered electron images after different milling times

Milling time (h)	Atomic percent	
	Mg	Ni
2	100	–
10	98	2
40	91	9
70	74	26

The calculation of the heat flow as a function of milling time was done for the first exothermal event. Values obtained are 5.4 and 14.4 J g^{-1} for 30 and 70 h of processing, respectively. As milling progresses, heat flow values increase and pass to a maximum reaching 43.2 and 45.6 J g^{-1} at 100 and 150 h, respectively. Values decrease at long milling times leading to a 40.8 J g^{-1} at 200 h. The wide temperature range of the second exothermic event makes difficult both the calculation of the heat flow and the selection of the baseline.

To clarify the origin of the two exothermal reactions, a combination of DSC experiments run up to a temperature above each thermal event followed by samples withdrawal and further XRD analysis was carried out. Two sets of samples were selected for this analysis based on the identity of the phases present in the starting material. Samples treated during 100 and 200 h of MA, referred to as MA100 and MA200, were chosen. Their phase compositions are shown in Table 1 and Fig. 1, respectively.

Two exothermal peaks centered near 133 and 237 °C are exhibited in the DSC curve of MA100 sample displayed in Fig. 3. The starting phases are nanocrystalline Mg and crystalline Ni as shown in XRD patterns of Fig. 4. After heating up to 160 °C, an improvement of the Mg crystallinity and formation of Mg_2Ni are observed in agreement with data shown in Table 3. Crystallite size of Mg is increased from 25 to 44 nm and nanocrystalline Mg_2Ni is formed due to heating. At the same time, a reduction of the broad peak in the $2\Theta = 35–40°$ region is clearly observed. These results are correlated to two simultaneous processes present within the first reaction during annealing.

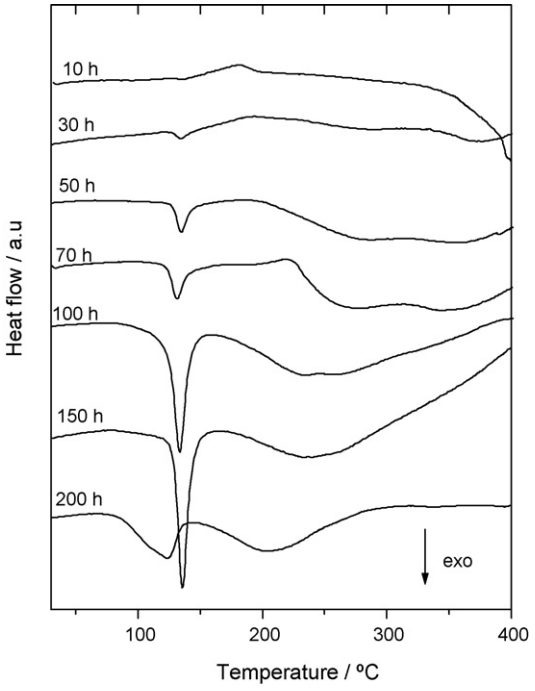

Fig. 3. DSC curves of mixture 2Mg–Ni after MA as a function of milling time.

Table 3
Evolution of the crystallite (average) size d (nm) and average strains (%) of the different phases after annealing

Sample	Temperature (°C)	Mg		Ni		Mg_2Ni	
		d (nm)	Strain (%)	d (nm)	Strain (%)	d (nm)	Strain (%)
MA100	–	25	10	49	4	–	–
	160	44	6	50	4	20	25
	300	115	2	74	2	50	9
	400	–	–	–	–	161	2
MA200	–	–	–	27	8	16	28
	140	22	11	41	7	15	29
	300	–	–	–	–	32	14
	400	–	–	–	–	73	6

The first one is the crystallization into crystalline Mg_2Ni of an amorphous Mg-rich phase formed during milling of composition shown in Table 2. The second one involves the grain growth and strain relaxation of Mg. The heat flow value calculated for this first exothermic peak is 5.4 J g^{-1}.

Phase composition changes are observed after withdrawal of samples at temperatures higher than the ending of the second exothermic broad peak. Extra Mg_2Ni formation correlated to an increase of their peak intensities and a simultaneous decrease of the diffraction lines of Ni and Mg are revealed by XRD analysis performed at this temperature as shown in Fig. 4. Complete formation of Mg_2Ni and total disappearance of both Ni and Mg are observed after heating at 400 °C. Therefore, the second reaction peak shown in Fig. 3 is partially associated with thermal activated reaction between the residual Mg and Ni phases.

XRD patterns of MA200 composed mainly of Mg_2Ni and Ni nanocrystalline are shown in Fig. 5. After annealing up to 140 °C, a transformation of some sample material into crystalline Mg_2Ni and remaining Ni is observed. Mg peaks become clearly observed, Ni crystallite size increases and Mg_2Ni size remains close to values of 15 nm. Two processes related to the first exothermic peak are evidenced by the analysis of the DSC scans and XRD patterns. The first is the crystallization of Mg_2Ni from an amorphous phase precursor and the second is the simultaneous grain growth and strain relaxation of Mg and Ni. The minor amount of heat flow (40.8 J g^{-1}) associated with the first thermal event is due to the partial crystallization of Mg_2Ni from amorphous Mg-rich phase during long milling. The disappearance of Mg and Ni phases related to the complete Mg_2Ni formation is due to subsequent heating up to 300 °C. Then, it is possible the synthesis of Mg_2Ni via a combined MA for 200 h followed by non-isothermal heating up to 300 °C. These are milder conditions respect to previous work using low energy mill [17]. Unlike that case, total formation of Mg_2Ni is observed in MA100 after non-isothermal heating up to 400 °C as shown in Fig. 4.

The mechanism of MA process of the 2Mg–Ni mixture can be deduced from systematic analysis of XRD, DSC and SEM/EDX data. Although the refinement of each metal is different, size of both Mg and Ni grains are progressively reduced during the first hours of milling. As this process progresses, Mg peaks become broader than those of the initial sample. It is associated not only to a strong crystallite size reduction and strain increase but also to the formation of an amorphous phase revealed by a background peak in the $2\Theta = 35–40°$ region. The existence of a Mg-rich phase which Ni content is increased as milling progresses is corroborated by EDX analysis. The heat flows of simultaneous

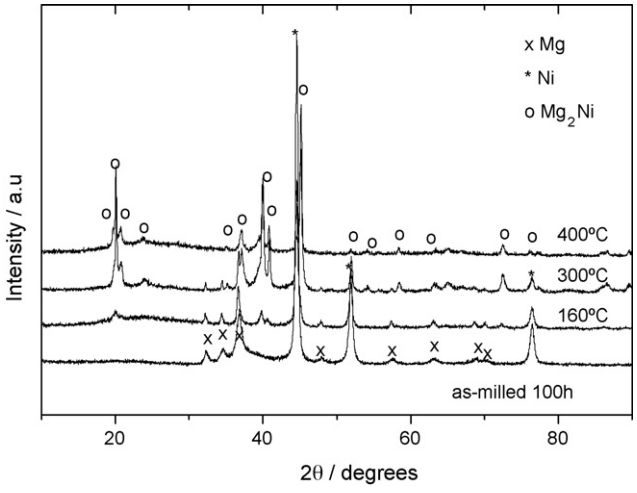

Fig. 4. XRD patterns of MA100 as-milled sample and after DSC runs stopped at 160, 300 and 400 °C.

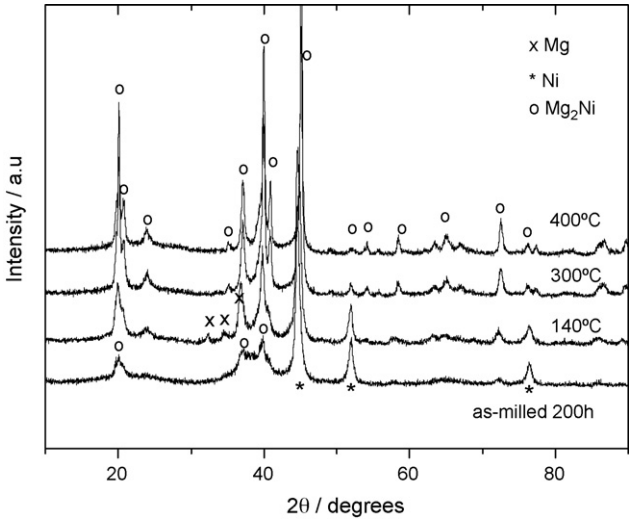

Fig. 5. XRD patterns of MA200 as-milled sample and after DSC runs stopped at 140, 300 and 400 °C.

amorphous phase crystallization and grain growth–relaxation processes were calculated from DSC runs. The values are practically 0 for 10 h which in turn is related to the absence of the amorphous phase and about 43 J g^{-1} for 100 h. Since the crystallite sizes of Mg and Ni are 18 and 43 nm after 150 h of milling, the refinement evolution of the first metal is much faster than the second one. It is in agreement with previous results [15,16] and also with predictions in relation with their crystallographic structures [23].

Amorphous Mg-rich and crystalline Ni phases along as nanocrystalline Mg_2Ni with average crystallite size of 16 nm is produced by further milling up to 200 h. Nevertheless, no complete Mg_2Ni formation is reached during MA, and residual Ni is still detected after 320 h of milling. The crystallization of the amorphous phase formed during milling is induced by low temperature annealing lower than 150 °C.

Both minimal unreacted Mg and Ni crystalline phases and close to maximum amorphous phase amounts are related to highest heat flow measurements after 100–150 h of milling. The crystallization of the amorphous phase and fractional sample transformation to Mg_2Ni is performed under milling evolution. Solid-state interdiffusion reaction between Ni and Mg particles is achieved during subsequent heating up to 300 °C. Since most of the sample was already transformed into Mg_2Ni by milling, the heat flow evolved from DSC runs is smaller. Full Mg_2Ni formation with crystallite size of 32 nm is the effect of annealing up to 300 °C. Therefore, grain growth for the sample milled 200 h and annealed up to 300 °C is not substantial. It is concluded that MA followed by annealing is an appropriate technique to produce stable nanocrystalline Mg_2Ni microstructures at 300 °C.

Moreover, experimental evidence of the processes present during thermal evolution of sample is summarized in Table 3. First exothermal event is associated to grain growth and strain relaxation during crystallization of Mg-rich amorphous phase to form Mg_2Ni, while second thermal event is correlated to solid–solid Mg–Ni interdiffusion. The contribution of grain growth and relaxation processes on both exothermal events was not demonstrated before [14–16].

Clear evidence of the formation of nanocrystalline Mg_2Ni during low temperature annealing is provided by this thermal–structural study. It has two different relevant consequences. Firstly, it is possible to produce Mg_2Ni by combination of low energetic mechanical milling followed by non-isothermal heating up to 300 °C. Secondly, interesting absorption–desorption properties are expected for nanocrystalline Mg_2Ni. Since sorption kinetics of Mg-based alloys is diffusion limited and it can be very fast in the grain boundaries with an occupancy of up to 30% of the total volume of nanocrystalline powders, absorption and desorption rate should be improved. The sorption properties of the MA200 sample are studied at 300 °C in the following section.

3.2. Hydrogen storage properties

Dynamics absorption and desorption PCIs at 300 °C of the MA200 sample are shown in Fig. 6. An extended plateau with the pressure increase is exhibited by the first absorption cycle

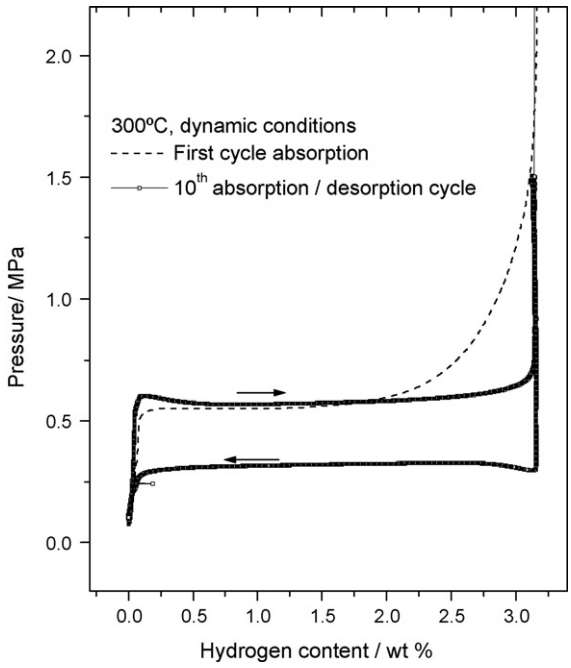

Fig. 6. Pressure–composition absorption/desorption curves at 300 °C for MA200 composite.

due to the transformation of Mg_2Ni to Mg_2NiH_4. After 10 cycles of absorption/desorption a flat plateau at 0.57 MPa is obtained. It is extended up to 3.2 wt% of hydrogen. It is known that upon cycling the sample suffers particle size reduction and pulverization of the material, which favors the hydriding process. During the 10th desorption cycle a flat plateau at about 0.32 MPa can be identified, showing the previously reported hysteresis in the Mg–Ni–H system [3]. The data of the plateau pressure are similar to those reported for Mg_2Ni produced from both metallurgical processes [3] and nanoparticles [22]. The most remarkable result is the good absorption capacity observed without activation process from the first cycle.

To characterize the hydrogen sorption kinetics of nanocrystalline MA200 sample, the temperature dependence was studied as shown in Fig. 7. Initial hydrogen pressure selected was 2.9 MPa. Very fast hydrogen absorption rates were observed at temperatures between 150 and 300 °C as displayed in Fig. 7A. Two different steps are present during hydrogen absorption curves. The first one occurs in less than 100 s, while the second one involves longer times. This behavior can be related to the presence of a lot of crystallite boundaries produced under milling. These boundaries act as fast diffusion paths for hydrogen atoms. These defects created on the surface of the mechanically synthesized material can play the role of the nucleation sites for the formation/decomposition of Mg_2NiH_4 during the absorption/desorption cycles. Similar behavior and absorption rate were observed during hydrogen absorption for nanocrystalline Mg_2Ni synthesized from a hydrogen plasma–metal reaction [24,25] and from nanocrystalline Mg_2Ni produced by high energy MA [6]. Although the driving force for hydrogenation increases, the total hydrogen storage capacity decreases as temperature does as shown in

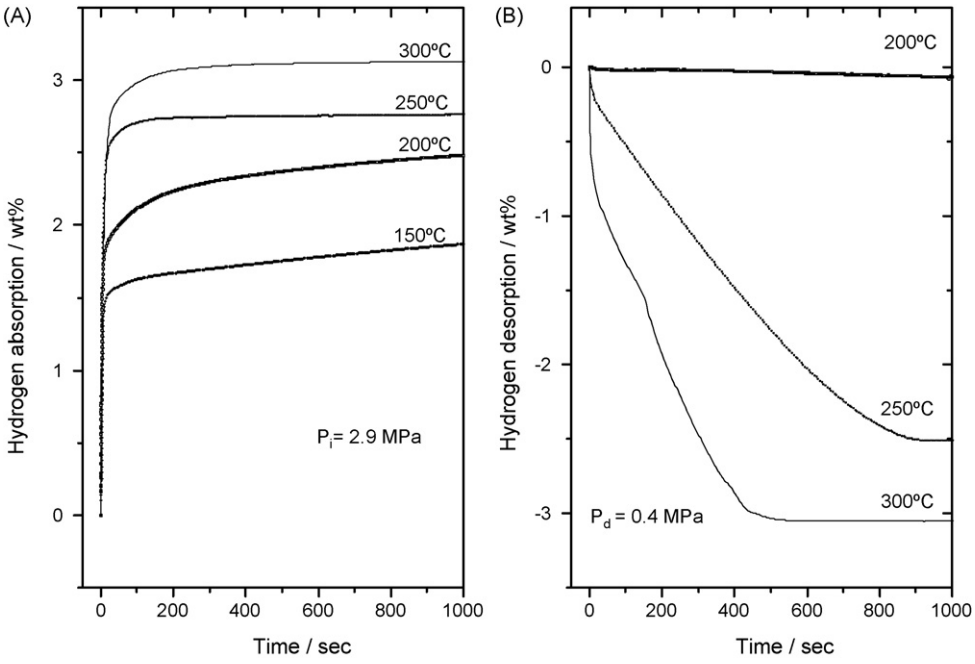

Fig. 7. Hydrogen (A) absorption and (B) desorption of MA200 composite at different temperatures. Initial hydrogen pressure during absorption, $P_i = 2.9$ MPa; desorption pressure, $P_d = 0.4$ MPa.

Fig. 7A. This phenomenon was observed and analyzed before under equilibrium conditions [26]. Then, the reaction rate seems not to be dominated by thermodynamic driving force. Moreover, the kinetic analysis should consider the occurrence of LT–HT hydride phase transition near 250 °C, and the difficulty to produce the LT modification under moderate experimental conditions [11]. Additional measurements must be performed to clarify the contribution of each step on the total hydrogen absorption rate.

Hydrogen desorption from hydride MA200 composite is illustrated by curves in Fig. 7B. At 250 °C, desorption rate is fast and 1000 s are enough to desorbed 3 wt% of hydrogen. On the contrary, hydride decomposition was practically non-detectable at 200 °C in agreement with DSC measurement (not shown). Results in the literature indicate that desorption times of Mg_2Ni milled are typically 1500 s at 250 °C [9]. Therefore, it seems that longer milling leads to better kinetics for Mg_2Ni by creation of activated surface, crystallite boundaries, defects and other nanocrystalline characteristics.

4. Conclusions

Mechanical alloying of the 2Mg–Ni mixture using a low energetic mill was carried out. The milling during the first 100 h leads to the formation of nanocrystalline Mg, crystalline Ni and a Mg-rich amorphous phase. Nanocrystalline Mg_2Ni is produced after 200 h of milling, simultaneously with Mg-rich amorphous phase and Ni. The formation of an amorphous Mg-rich phase during milling was demonstrated by using systematic XRD, DSC and SEM/EDX analysis. A combination of low energetic mechanical alloying and heating up to 300 °C under argon allows the synthesis of homogenous and nanocrystalline Mg_2Ni powders. Crystallization of Mg-rich amorphous phase and simultaneously crystallite growth–strain relaxation of Mg and/or Ni is produced by annealing at 300 °C. Nanometer Mg_2Ni is obtained during heating up to 300 °C with a final crystallite size of about 30 nm.

Nanocrystalline Mg_2Ni synthesized by combined milling–annealing procedure is stable on hydriding/dehydriding cycling. Readily hydrogen absorption during the first cycle without activation is obtained for this material. Absorption kinetics at 200 °C is better than that of MA nanocrystalline Mg_2Ni reported in previous works. Desorption rate is slightly improved at 250 °C compared to high energy mechanical alloyed Mg_2Ni. The good sorption properties are associated with the particular nanostructure of Mg_2Ni, which is dependent of the mechanochemical history and annealing temperature.

Acknowledgments

The authors thank CONICET, ANPCyT and TWAS (Third World of Academy of Sciences) for partial financial support to carry out this work.

References

[1] T. Massalski, H. Okamoto, P. Subramanian, L. Kacprzak (Eds.), Binary Alloy Phase Diagrams, second ed., American Society for Metals, Metals Park, OH, 1990, p. 2529.
[2] P. Selvam, K. Yvon, Int. J. Hydrogen Energy 16 (1991) 615–617.
[3] J.J. Reilly, R.H. Wiswall, Inorg. Chem. 7 (1968) 2254–2256.
[4] P. Zolliker, K. Yvon, C.H. Baerlocher, J. Less Common Met. 115 (1986) 65–78.
[5] D. Noréus, L. Kihlborg, J. Less Common Met. 123 (1986) 233–239.
[6] L. Zaluski, A. Zaluska, J.O. Ström-Olsen, J. Alloys Compd. 217 (1995) 245–249.
[7] L. Lü, M.O. Lai, Mechanical Alloying, Kluwer Academic Publishers, Boston, 1998.

[8] J.H. Huot, E. Akida, T. Takada, J. Alloys Compd. 231 (1995) 815–819.
[9] G. Liang, J. Huot, S. Boily, A. Van Neste, R. Schultz, J. Alloys Compd. 282 (1999) 286–290.
[10] A.K. Singh, A.K. Singh, O.N. Srivastava, J. Alloys Compd. 227 (1995) 63–68.
[11] L. Zaluska, A. Zaluski, J.O. Ström-Olsen, J. Alloys Compd. 253 (1997) 70–79.
[12] J. Chen, S.X. Dou, H.K. Liu, J. Alloys Compd. 244 (1996) 184–189.
[13] M. Abdellaoui, D. Cracco, A. Percheron-Guegan, J. Alloys Compd. 268 (1998) 233–240.
[14] T. Spassov, P. Solsona, S. Suriñach, M.D. Baró, J. Alloys Compd. 349 (2003) 242–254.
[15] P. Rojas, S. Ordóñez, D. Serafini, A. Zúñiga, E. Lavernia, J. Alloys Compd. 391 (2005) 267–276.
[16] T. Spassov, P. Solsona, S. Bliznakov, S. Suriñach, M.D. Baró, J. Alloys Compd. 356/357 (2003) 639–643.
[17] L. Aymard, M. Ichitsubo, K. Uchida, E. Sekreta, F. Ikazaki, J. Alloys Compd. 259 (1997) L5–L8.
[18] F. Castro, F.C. Gennari, J. Alloys Compd. 375 (2004) 292–296.
[19] F.C. Gennari, F.J. Castro, J. Alloys Compd. 396 (2005) 182–192.
[20] I. González Fernández, G.O. Meyer, F.C. Gennari, J. Alloys Compd. 446–447 (2007) 106–109.
[21] S. Enzo, E. Bonetti, I. Soletta, G. Cocco, J. Phys. D: Appl. Phys. 24 (1991) 210–216.
[22] G. Meyer, D.S. Rodríguez, F. Castro, G. Fernández, Hydrogen Energy Progress, Proceedings of the 11th World Energy Conference, vol. 2, Stuttgart, 1996, pp. 1293–1297.
[23] H. Fecht, E. Hellstern, Z. Fu, W. Johnson, Metall. Trans. A 21A (1990) 2333–2337.
[24] H. Shao, H. Xu, Y. Wang, X. Li, Nanotechnology 15 (2004) 269–274.
[25] H. Shao, Y. Wang, H. Xu, X. Li, J. Solid State Chem. 178 (2005) 2211–2217.
[26] T. Kuji, H. Nakano, T. Aizawa, J. Alloys Compd. 330–336 (2002) 590–596.